Thermal, structural and photophysical properties of the organic semiconductor Alq3

Michael Cölle, Wolfgang Brütting

Thermal, structural and photophysical properties of the organic semiconductor Alq$_3$

M. Cölle[*,1] and **W. Brütting**[**,2]

[1] Universität Bayreuth, Experimentalphysik II and Bayreuther Institut für Makromolekülforschung (BIMF), 95440 Bayreuth, Germany
[2] Universität Augsburg, Experimentalphysik IV, 86135 Augsburg, Germany

This review describes the thermal, structural and photophysical properties of different polycrystalline phases of the organic semiconductor Alq$_3$. In particular the new blue luminescent $\square$-phase is shown to contain the facial isomer. The results obtained by using differential scanning calorimetry, X-ray diffraction, infrared spectroscopy, transient and delayed photoluminescence measurements clearly demonstrate the existence of this isomer. From the results presented it is now possible to obtain the pure facial isomer of Alq$_3$ in large quantities, providing the basis for further investigations to determine its effects on the performance of organic light-emitting diodes. Furthermore, recent results on the properties of the triplet states in Alq are presented. This includes the population of the electronic excited triplet state due to inter-system crossing and the spectrum of the phosphorescence.

1 Introduction

8-hydroxyquinoline metal chelate complexes were used for many years in analytical chemistry for a gravimetric determination of various metal cations in solution [1]. The development of more convenient spectroscopic techniques has meanwhile replaced this method and concomitantly decreased the interest of researching chemists in this reagent. Increasing interest in tris(8-hydroxyquinoline)aluminum(III) (Alq$_3$) shown in Fig. 1 for technical applications started with a report on efficient electroluminescent devices using Alq$_3$ as the active medium [2]. These so-called organic light emitting diodes (OLEDs) opened the way for a new generation of flat panel displays. After nearly two decades of intensive research and development of OLEDs, Alq$_3$ still continues to be the workhorse in low-molecular weight materials for these devices. It is used as electron-transporting layer, as emission layer where green light emission is generated by electron-hole recombination in Alq$_3$, and it also serves as host material for various dyes to tune the emission color from green to red [3]. Many studies in this field have focused on the optimization of device performance with respect to efficiency and long-term stability or on the understanding of charge transport properties of amorphous thin films [4–13]. These investigations revealed that electrical transport in Alq$_3$ is characterized by a hopping-type charge carrier mobility displaying a Poole–Frenkel-like dependence on the electric field and on temperature. It was further found that trapping in distributed trap states is involved in charge transport, in particular at low fields. Different suggestions as to the origin of these traps were made, including a polaronic self–trapping effect, extrinsic traps due to impurities and the presence of a mixture of isomers of the Alq$_3$ molecule having different energy

---

[*] Corresponding author: e-mail: info@michael-coelle.de, Phone: +49 921 55 26 02, Fax: +49 921 55 2621
[**] e-mail: wolfgang.bruetting@physik.uni-augsburg.de

1096
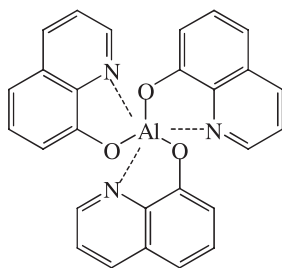
Fig. 1 Chemical structure of Tris(8-hydroxyquinoline)aluminum(III) (Alq$_3$).

levels. However, no clear proof for one or other possibility explaining the microscopic nature of these traps was given.

Another surprising circumstance was that in spite of the widespread usage of Alq$_3$ as amorphous films in OLEDs, comparatively few investigations were devoted to the material's structural, electronic and optical properties in the crystalline state, as well as to the dependence of these properties on the preparation conditions until recently [14–17]. On the other hand, it was mentioned in one of the very first publications on OLEDs based on thin films that the so-called "amorphous" film of Alq$_3$ might have nanocrystalline domains [2], which raises questions concerning the morphology and properties of Alq$_3$. For example, what kind of crystalline phases can be formed by Alq$_3$ and what are their electronic and optical properties? What is the packing of the molecules? Packing and intermolecular interactions are important for optical properties as well as for their electrical characteristics and the transport mechanism of charge carriers.

Another unresolved issue concerns the isomerism of the Alq$_3$ molecule. It is well-known that octahedral complexes of the type MN$_3$O$_3$, where M is a trivalent metal and N and O stand for the nitrogen and oxygen atoms in the quinoline ligands, can occur in two different geometric isomers: meridional and facial, as shown in Fig. 2 [18]. Nevertheless, until recently only the meridional isomer had been clearly identified and no direct experimental evidence for the facial isomer had been found. Therefore it was generally believed that the meridional isomer is predominant, both in amorphous films and crystals of Alq$_3$. The existence and the properties of the facial isomer are discussed in detail in the literature and a key issue is its possible presence in sublimed Alq$_3$ films [14, 19–27]. Many suggestions have been made about its influence on trap density, charge carrier transport and thus on the characteristics and performance of OLEDs. For example, the higher dipole moment of the facial isomer is expected to influence the
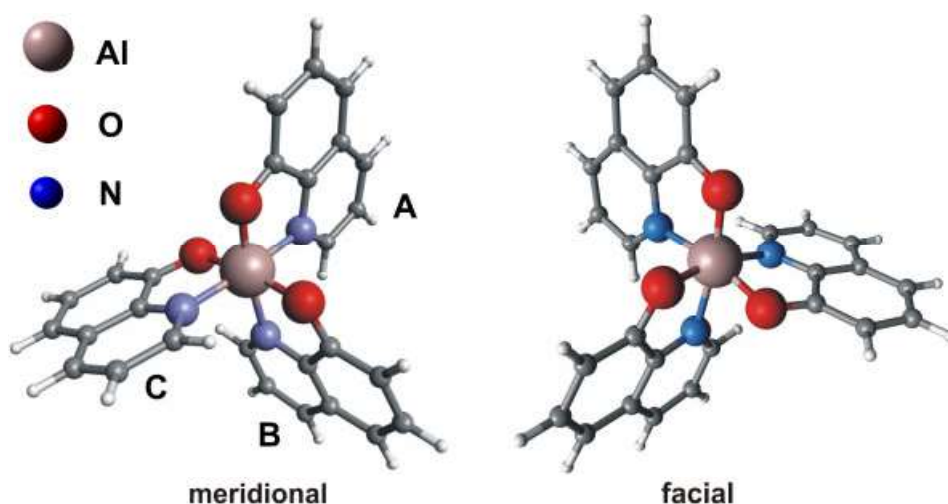
Fig. 2 Molecular structure of the meridional and facial isomer of Alq$_3$. For the facial isomer the ligands are equivalent, but in the meridional molecule the ligands can be clearly distinguished and therefore the labeling of the ligands by A, B and C is given.

morphology of the film as well as the injection of charge carriers at the interface. In addition the different HOMO and LUMO levels predicted for the two isomers are expected to influence the injection barrier and could act as traps for charge carriers [24, 28–32]. Therefore the question is whether the facial isomer is present in one or other modification of Alq$_3$, and if so, if it is possible to isolate it. The isolation of the facial isomer is of great interest, as it will allow its properties to be examined separately and thus its role in OLEDs to be clarified.

2 Crystalline phases of Alq$_3$

This section describes the preparation and identification of different crystalline phases of Alq$_3$ obtained by sublimation. In order to induce growth of different phases, the temperature gradient in a sublimation tube was used. Phases that grow at different temperatures were obtained and their crystal structures were investigated.

Temperature gradient sublimation is a common method for purification of organic materials. After this purification procedure polycrystalline powders of different appearance were found in the sublimation tube and thus we distinguished between three different zones in the glass tube. The materials in these zones, hereafter called fractions, differ in their shape of crystals, their color, their solubility and their fluorescence.

A typical example of these glass tubes after sublimation is shown in Fig. 3 with indicated areas for the three different fractions. In the hottest zone of the growth area there is an approximately 1.5 cm wide region with very small needle-like crystals with white or slightly yellow appearance (fraction 1). This zone is followed by the main fraction (about 8.5 cm) with yellow cubic crystals and dimensions up to $500 \times 500 \times 500 \ \mu m^3$, showing yellowish-green fluorescence (fraction 2). In the subsequent colder zone of the sublimation tube another fraction is obtained with dark yellow-green needle-like crystals with a size of $50 \times 50 \times 500 \ \mu m^3$ (fraction 3).

These fractions have different solubility in organic solvents. While fraction 3 and (apart from a small residue) also fraction 2 are readily dissolved in chloroform at a relatively high concentration of more than 1% by weight, the solubility of fraction 1 is extremely poor. It takes several hours to dissolve a sizeable amount in chloroform, but then the color of the solution becomes similar to that of the other fractions.
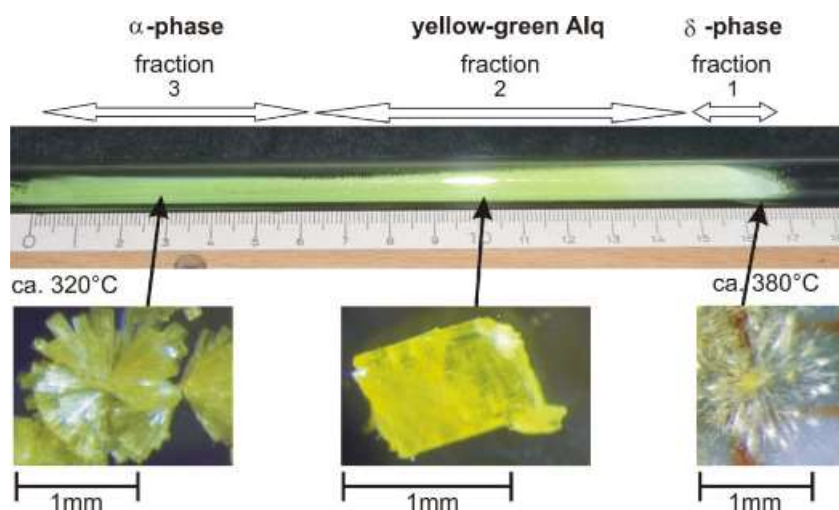
Fig. 3 Picture of a sublimation tube. Due to the temperature gradient in the sublimation tube, the material obtained is separated into three zones, which are labeled by fraction 1, fraction 2 and fraction 3. Crystals of these fractions in the tube are also shown.
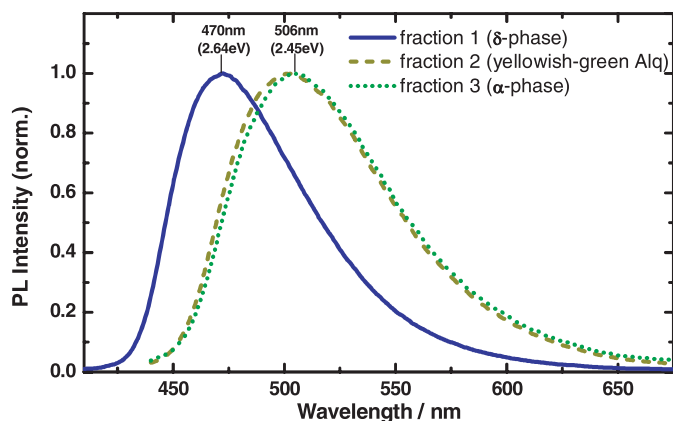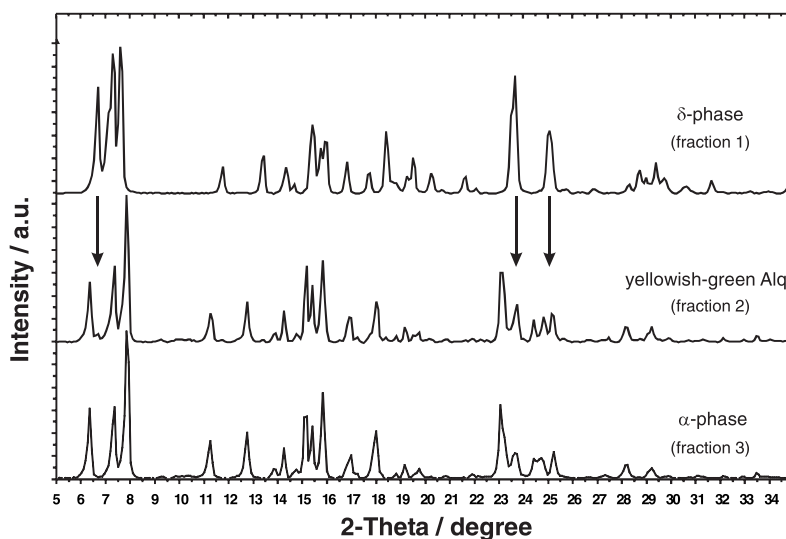
Fig. 4 PL spectra of the three fractions obtained from the sublimation tube, excited at 350 nm and measured at room temperature.

Further differences between the three fractions are found in their photoluminescence (PL) spectra. Figure 4 shows the spectra measured with an excitation wavelength of 350 nm at room temperature. All fractions show one broad PL band with no additional structures and a tail at the side of longer wavelengths. Their main difference is the large blue shift of the PL maximum of about 0.19 eV (36 nm) from fraction 3 to fraction 1 with a PL maximum at about 506 nm (2.45 eV) and 470 nm (2.64 eV), respectively.

In order to investigate the origin of these differences, the crystallographic data of the three fractions were determined by using X-ray powder diffraction as shown in Fig. 5. As a result two different phases were found. Fraction 1 and fraction 3 show the main differences. These differences are best seen for small angles below 9 degrees and in the region between 22 and 26 degrees. From these two spectra the unit cells for fraction 1 and fraction 3 were determined. Indexing of the peaks observed is given in Ref. [15] and [17] and the cell parameters determined for the different phases of Alq_3 are summarized in Table 1 together with two other phases (β- and γ-) found by Brinkmann et al. The spectrum of fraction 2 seems to be a mixture of two phases. Basically the spectrum is similar to that of fraction 3 apart from some small peaks or shoulders at positions where fraction 1 and fraction 3 are different, for example at 23.5 degrees and especially at 6.69 degrees. This suggests that fraction 2 mainly consists of the same phase as fraction 3, but has some small admixtures of material from fraction 1. The result that fraction 2 is a mixture of two different phases is relevant for applications, as it is mainly this fraction that is used for fabrication of OLEDs. From this X-ray data it becomes clear that the main difference is between fraction 1 and fraction 3, which have different unit cells given in Table 1.

Table 1 Crystallographic data of the polycrystalline phases of Alq_3.

	α-phase (fraction 3) [14, 15]	-phase [14]	γ-phase [14]	-phase (fraction 1) [16, 17]
crystal system	triclinic	triclinic	trigonal	triclinic
space group	P-1	P-1	P-31c	P-1
Z	2	2	2	2
a [Å]	12.91	10.25	14.41	13.24
b [Å]	14.74	13.17	14.41	14.43
c [Å]	6.26	8.44	6.22	6.18
α [°]	89.7	97.1	90	88.55
β [°]	97.7	89.7	90	95.9
γ [°]	109.7	108.6	120	113.9
V [Å³]	1111	1072	1118	1072.5

Fig. 5 X-ray powder diffractograms of polycrystalline Alq$_3$ fractions 1, 2, and 3 obtained from the sublimation tube in the 2θ-range from 5 to 35 degrees (step width $\Delta 2\theta = 0.083°$). Arrows mark areas with the most significant differences.

It is possible to compare these crystal data obtained above with results of other researchers. Brinkman et al. reported on three different crystalline structures called α-, β- and γ-phase [14]. The published data for the α-phase are identical to those of fraction 3. β-Alq$_3$ is grown from solution and its properties are in principle similar to the α-phase, only with a small red shift in the PL due to slightly different intermolecular interaction in the crystal. The published data of γ-Alq$_3$ are listed in Table 1 for completeness, although they have to be considered as preliminary data and refined or improved data are going to be published [33]. All phases and evaporated films were identified as consisting of the meridional isomer, and therefore only the meridional molecule was found at that time.

The denotation of the phases in our work is in accordance with these published data. Fraction 3 and the main part of fraction 2 consist of the α-phase. The structure of fraction 1 is new and no corresponding phase has been published so far. Accordingly fraction 1 is hereafter called the δ-phase of Alq$_3$.

δ-Alq$_3$ exhibits major differences to all other phases obtained from the sublimation tube. It is a whitish powder, has a different crystal structure and, importantly, a strongly blue-shifted PL. On the other hand the α- and β-phase are very similar, as reported by Brinkmann et al. Consequently it seems to be most interesting to investigate the differences and similarities of the α- and δ-phase of Alq$_3$, as will be done in the following sections of this article.

3 Thermal properties of Alq$_3$

The phases discussed above were grown in different areas of the sublimation tube in regions of different temperature. Thus temperature obviously has a strong influence on the formation of these phases and it is important to learn more about the thermal properties of Alq$_3$. Therefore the formation conditions of the different phases of Alq$_3$ were investigated using differential scanning calorimetry (DSC) measurements in combination with structural and optical characterization.

Figure 6 shows the DSC measurement of polycrystalline Alq$_3$ powder (α-phase) taken at a heating rate of 20 °C/min. Coupled endothermic and exothermic peaks are observed at about 395 °C prior to the large melting transition at 419 °C. This additional phase transition has also been reported in the literature and has been attributed to polymorphism of the crystalline material [14, 34]. It is very pronounced at fast heating rates (above 15 °C/min). For slow heating rates the endothermic and exothermic transitions be-
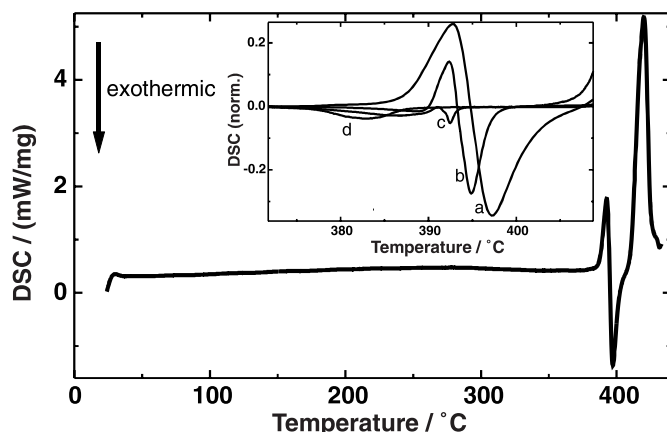
Fig. 6 DSC trace of Alq$_3$ with pronounced thermal transitions at 393°, 396° and 419 °C measured at a heating rate of 20 °C/min. Inset: Broadening and intermingling of the endothermic and exothermic peaks around 395 °C in the DSC signal related to the sweep speed (a: 20 °C/min, b: 10 °C/min, c: 5 °C/min, d: 2 °C/min; normalized on the melting peak intensity). At low measuring speed only the more pronounced exothermic transition is visible.

come broader and the peak height decreases as compared to the strong melting peak. The peaks start to intermingle and are shifted to a slightly lower temperature, as shown in the inset of Fig. 6 for heating rates of 20°, 10°, 5° and 2 °C per minute. This behavior is similar to known irreversible monotropic solid-solid transitions [35–37]. Typically, the monotropic transition is slow and is mostly observed a few degrees below the melting point. Thus it is advisable to measure the monotropic transition isothermally at very slow heating rates.

It should be noted that increasing the temperature above 430 °C results in decomposition of the material and that a small broad transition at 320 °C reported by Sapochak et al. [34] was not observed in our samples. For the following measurements a slow heating rate of 2 °C/min was used, where the shift of the peak temperatures is fairly small (see Fig. 6) and where it is possible to stop the process at a defined temperature. Using this procedure the conditions for the preparation of different Alq$_3$ phases by a controlled thermal annealing process were investigated.
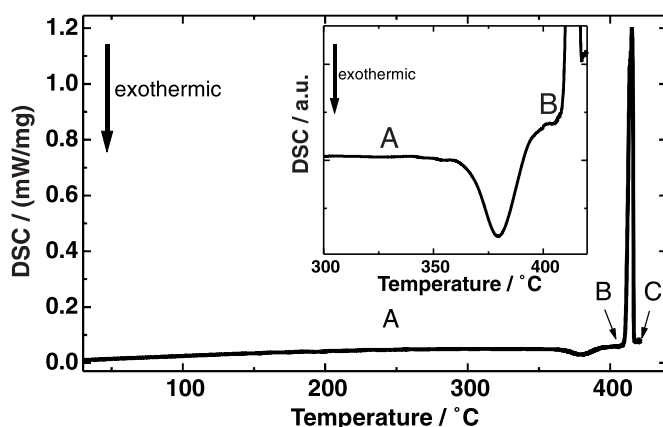
Fig. 7 DSC trace of Alq$_3$ measured at a heating rate of 2 °C/min. The clearly pronounced exothermic phase transition at 380 °C prior to the melting point is enlarged in the inset, as it becomes broad and less intense compared to the melting peak for this slow heating rate. A, B and C mark the regions of yellowish-green Alq$_3$, blue Alq$_3$ and melt, respectively.
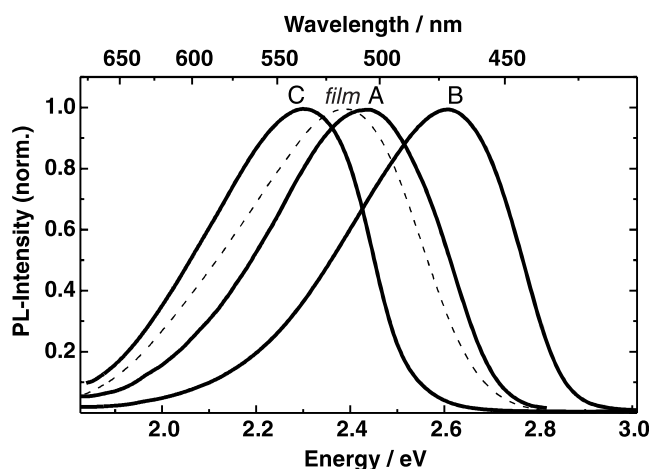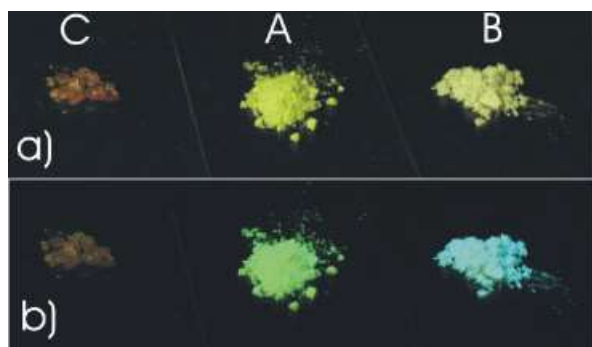
Fig. 8 PL spectra of Alq$_3$ samples taken from regions A, B and C of Fig. 7, respectively, excited at 350 nm. The PL of an evaporated Alq$_3$ film (dashed line) is shown for purposes of comparison. All spectra were measured at room temperature.

For these slow DSC measurements three different regions are distinguished in Fig. 7. In the first region (A) below the exothermic phase transition Alq$_3$ is the usual yellowish green powder, in the second region (B) between this phase transition and the melting peak Alq$_3$ is a whitish powder, and finally in region C Alq$_3$ is a liquid melt. The glassy state of Alq$_3$ was obtained by quenching this melt in liquid nitrogen. Its highly amorphous character was verified by using X-ray powder diffraction measurements with an image plate detection system. Cooling down the liquid melt slowly resulted in yellowish-green powder (A) again, as was previously reported [38]. All of these materials are stable at room temperature.

Figure 8 shows the PL spectra measured at room temperature of annealed polycrystalline Alq$_3$ powder from regions A and B as well as of the quenched amorphous melt (C). For annealing temperatures up to 365 °C Alq$_3$ is a yellowish-green powder with a PL maximum at 506 nm (curve A). After the exothermic transition at about 380 °C, there is a big blue shift of 0.18 eV (37 nm), associated with a slight change in the shape of the PL spectrum (curve B), which is less symmetric for blue Alq$_3$. The quenched melt (curve C) is clearly red-shifted (0.14 eV) compared to the yellowish-green Alq$_3$-powder (curve A). The strong difference in the emission color can be seen in Fig. 9, where samples of the quenched melt, yellowish-green and blue Alq$_3$ are shown in daylight (a) and under UV-irradiation (b), respectively. The emission color is shifted from green (CIE coordinates: $x = 0.27$, $y = 0.5$) to blue ($x = 0.16$, $y = 0.26$). From Fig. 9 one can also see the relatively low PL intensity of the quenched melt compared to the very intense PL emission of blue Alq$_3$. For PL quantum efficiency the values obtained for blue Alq$_3$, yellowish-green powder, evaporated film and quenched amorphous melt were 51%, 40%, 19% and 3%, respectively.

For comparison the dashed line in Fig. 8 is the PL spectrum of an evaporated Alq$_3$-film as used in OLEDs. Although these films are commonly called "amorphous", one can clearly see that the PL maxi-

Fig. 9 Photographs of Alq$_3$ samples taken from regions A, B and C in Fig. 8: a) in usual daylight and b) under UV-irradiation (excitation wavelength: 366 nm), clearly showing the strong blue shift of the luminescence of the annealed material. (CIE color coordinates for A: $x = 0.27$, $y = 0.50$; for B: $x = 0.16$, $y = 0.26$).

1102
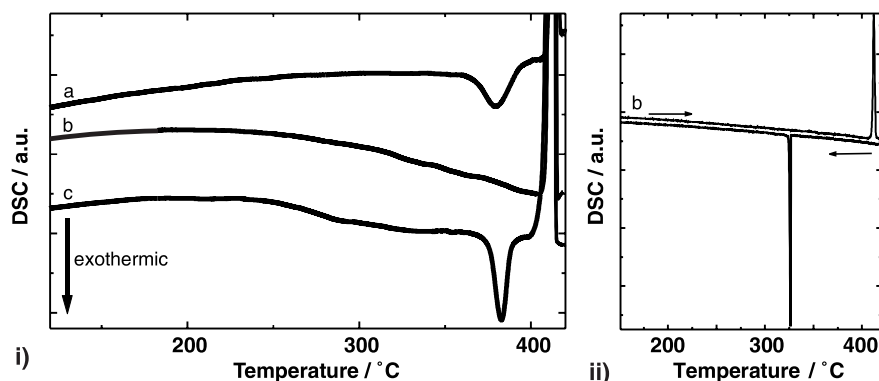
Fig. 10 DSC traces of a: yellowish-green Alq$_3$ and b: blue Alq$_3$. Trace c shows a second heating cycle after cooling down the melt (b) again. By annealing blue Alq$_3$ no phase transition at 380 °C is observed (trace b in i) and ii)). Cooling down the melt gives a strong recrystallization peak.

mum is located between the quenched melt and crystalline Alq$_3$. This is an indication of the nanocrystalline character of these films, as noted already by Tang et al. [2].

Yellowish-green Alq$_3$, blue Alq$_3$ and amorphous melt can be converted into each other. As described above, yellowish-green Alq$_3$ annealed above the phase transition at 380 °C results in blue Alq$_3$. Annealing blue Alq$_3$ above the melting point and cooling it down slowly, as shown in Fig. 10, yields yellowish-green powder again and a pronounced recrystallization peak is observed. With the same procedure of annealing the quenched melt above the melting point and cooling it down slowly, yellowish-green powder is obtained again, and the quenched melt is converted into blue Alq$_3$ by annealing it between 380 °C and 410 °C. The successful conversion from one phase into the other was confirmed by measurements of the PL spectra, FT-IR spectra, Raman spectra, and X-ray diffraction.

Obviously, blue Alq$_3$ is formed during the phase transition at about 380 °C. This phase transition appeared when starting the measurement with yellowish-green Alq$_3$, as shown in Fig. 10. On the other hand, when starting the annealing procedure with blue Alq$_3$ material no such phase transition was observed, as shown in Fig. 10i and ii trace b. However, measurements taken after the sample in Fig. 10b had cooled down showed the exothermic peak again, as can be seen in trace c of Fig. 10i.

As blue Alq$_3$ is formed in the region between the crystallographic phase transition and the melting point, the influence of temperature and preparation conditions in the region between 385 °C and 410 °C was investigated. Figure 11 shows X-ray powder diffraction spectra of blue Alq$_3$ prepared under three different conditions. For spectrum (I) yellowish-green Alq$_3$ powder (α-Alq$_3$) was annealed at 400 °C for 2 h. This spectrum is similar to the one obtained for fraction 1 in the sublimation tube shown in Fig. 5. The shoulder at $2\theta = 7.05°$ for different samples of blue Alq$_3$ was variably pronounced. From this one may assume another high-temperature phase to be present in these samples. To test this, Alq$_3$ was annealed for several minutes at a higher temperature of 410 °C (very close to the melting point) and a dark yellow substance was obtained, which exhibited only poor photoluminescence together with blue luminescent material. Its X-ray spectrum (Fig. 11 (II)) has a number of new peaks, which become very obvious for example at $2\Theta = 7.05°$ (the position of the shoulder in spectrum (I)) and 25.85°. On the other hand, spectrum (III) shows Alq$_3$-powder annealed at 390 °C for 6 hours. The additional lines observed in spectrum (II) are no longer present in this spectrum.

Based on these investigations, blue luminescent Alq$_3$ obtained by annealing yellowish-green Alq$_3$ (α-phase) above the phase transition at about 380 °C was identified as the δ-phase of Alq$_3$ with the unit cell given in Table 1. As seen in curves (I) and (II) of Fig. 11, annealing Alq$_3$ at temperatures higher than 380°, close to the melting point, results in the appearance of new peaks in the X-ray spectra, which can be attributed to an additional high temperature phase. Brinkmann et al. have reported on such a high temperature phase, namely γ-Alq$_3$ [14]. Using the given unit cell parameters from their work, the posi-
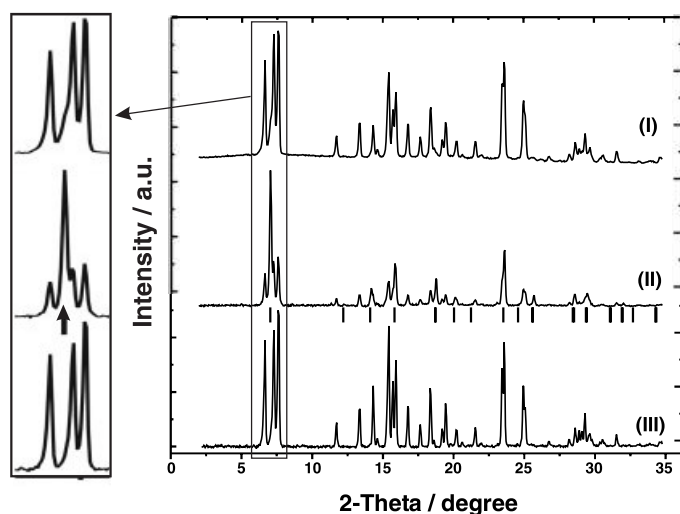
Fig. 11 X-ray powder diffractograms of polycrystalline blue Alq$_3$ prepared under different conditions. For spectrum (I) yellowish-green Alq$_3$-powder (α-Alq$_3$) was annealed at 400 °C for 2 hours. In spectrum (II) the powder was annealed at 410 °C (close to melting point). For spectrum (III) Alq$_3$ was annealed at 390 °C for 6 hours. The additional lines and shoulders observed in spectrum (II) are not present in spectrum (III). Bars in spectrum (II) mark calculated positions for all possible X-ray peaks of γ-Alq$_3$.

tions of all possible X-ray peaks for this phase were calculated, as indicated by the vertical bars in curve (II) of Fig. 11. These calculated peaks are located at the positions where spectrum (II) and (III) are different. Therefore it suggests that in sample (II) there is a high concentration of γ-Alq$_3$, whereas sample (III) is practically pure δ-Alq$_3$, as will be confirmed in the next section. From this it can be concluded that there are two high temperature phases of Alq$_3$: δ-Alq$_3$ and probably the γ-phase.

Blue luminescent Alq$_3$ obtained by train sublimation as described in the previous section and by annealing showed the same behavior with respect to its solubility as well as its properties in PL, DSC, and IR measurements, confirming that in both cases the δ-phase of Alq$_3$ was obtained. In the sublimation tube the different phases were separated due to the temperature gradient. Since δ-Alq$_3$ and the other high temperature phase (most likely γ-Alq$_3$) are formed in a relatively narrow temperature region, the separation of the two phases by train sublimation is difficult and a certain ratio of γ-Alq$_3$ is still present in the samples of δ-Alq$_3$, as indicated by the small shoulder at $2\theta = 7.05°$ in the X-ray spectrum. On the other hand, under appropriate annealing conditions it is possible to obtain pure δ-phase without any visible admixtures of other phases, as demonstrated in curve (III) of Fig. 11. A further advantage of this simple annealing process compared to temperature gradient sublimation is the possibility of obtaining large amounts (several grams) of pure δ-Alq$_3$ in a well-controlled process.

Chemical reactions during the annealing process can be excluded because the usual yellowish-green Alq$_3$ (α-phase) and the blue luminescent δ-Alq$_3$ can be easily converted into each other. Annealing yellowish-green Alq$_3$ at temperatures higher than 380 °C results in δ-Alq$_3$, while heating δ-Alq$_3$ above the melting point and cooling the melt down slowly results in yellowish-green powder again. Another method of reconverting blue Alq$_3$ into yellowish-green Alq$_3$ is to evaporate the material or to dissolve it in any appropriate solvent (e.g. chloroform). The same holds for the glassy state of Alq$_3$ obtained by quenching the melt. It is readily dissolved in chloroform and films of good quality can be cast from such solutions. The PL spectrum of such films is the same as for evaporated films of Alq$_3$. By annealing material in the glassy state, it is possible to obtain both the yellowish-green α-Alq$_3$ and the blue δ-Alq$_3$, depending on the temperature. In all cases pure Alq$_3$ with no visible contaminating material is obtained. The possibility of transforming Alq$_3$ from one phase into the other implies that even at these high tem-

peratures there is no decomposition or chemical reaction of the material. So it is important to emphasize that for all temperatures up to 425 °C we are dealing with Alq_3, in agreement with ^1H NMR and FT-IR analysis of Alq_3 annealed at 422 °C, where no decomposition products have been found [34]. By excluding chemical reactions the difference in the phases must be of physical and structural origin.

4 The molecular structure of δ-Alq₃

4.1 High resolution powder diffraction using synchrotron radiation

In the previous sections a new phase of Alq_3, the δ-phase, which exhibits major differences to all other phases, was introduced and characterized. Based on the observed blue-shift of the PL by almost 0.2 eV and the quantum chemical calculations of Currioni et al., which predicted a difference in the energy gap of the two isomers in that range, it could be supposed that the δ-phase contains the facial isomer of Alq_3. However, to prove this hypothesis it was necessary to resolve the crystal structure of the new phase, including the structure of the constituting molecules. The problem in determining the structure of organic molecular crystals is mainly due to the large number of atoms (104 for Alq_3) in the unit cell. Standard laboratory equipment requires single crystals to solve the structure of a new phase of a material; however, so far single crystals large enough for a full analysis of the structure have only been available for the β-phase of Alq_3 [14]. On the other hand, due to the use of high brilliance synchrotron radiation sources powder diffraction methods have progressed substantially in recent years, allowing very reliable determination of the structure from powder material without the need for larger single crystals. For this, high quality experimental data and specialized software for the analysis of the structure are required. These methods are very sensitive and unambiguous results are only to be expected if samples of one uniform crystal phase are measured. As the δ-phase can be isolated and δ-Alq_3 is easily obtained as a fine polycrystalline powder, these are good preconditions for this method.
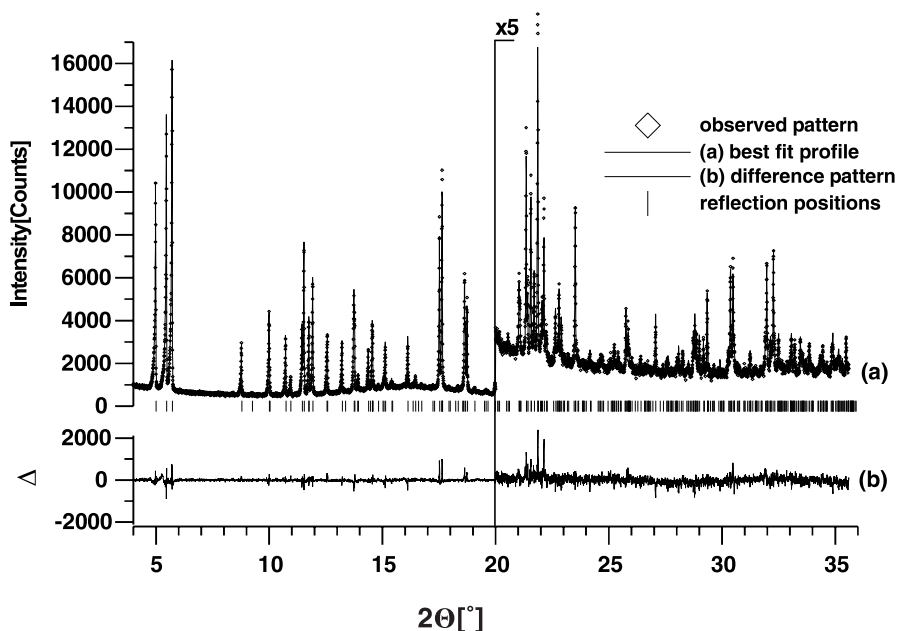
Fig. 12 Scattered X-ray intensity for ☐-Alq_3 under ambient conditions as a function of diffraction angle 2Θ. Shown are the observed patterns (diamonds), the best Rietveld-fit profiles on the assumption of a facial isomer (line) and the enlarged difference curves between observed and calculated profiles in an additional window below. The high angle part is enlarged by a factor of 5, starting at 20°. The wavelength was $\lambda = 1.15$ Å.

Table 2 Crystallographic data for δ-Alq$_3$. R_p, R_{wp}, and R–F^2 refer to the Rietveld criteria of the fit for profile and weighted profile respectively, defined by Langford and Louer [40].

| formula	Al(C$_9$H$_6$NO)$_3$	ρ-calc [g/cm^3]	1.423
temperature [K]	295	2Θ range [°]	4–35.7
formula weight [g/mol]	918.88	step size [°2Θ]	0.005
space group	P-1	wavelength [Å]	1.14982(2)
Z	2	μ [1/cm]	2.48
a [Å]	13.2415(1)	capillary diameter	0.7
b [Å]	14.4253(1)	R_p [%]	5.0
c [Å]	6.17727(5)	R_{wp} [%]	6.5
α [°]	88.5542(8)	R–F^2 [%]	10.5
β [°]	95.9258(7)	reduced χ^2	1.6
γ [°]	113.9360(6)	no. of reflections	337
V [Å^3]	1072.52(2)	no. of variables	115

In the case of a molecular crystal like Alq$_3$ it is necessary to start the simulation of the spectrum with an assumed configuration of the molecules within the unit cell in order to achieve convergence within a reasonable calculation time. Therefore we assumed a molecular configuration on the basis of the known connectivity of the molecule. The ligands were assumed to be planar and were randomly moved within a range of ±20° by a simulated annealing procedure until a minimal difference to the measured spectrum was obtained. After this, the position of the atoms was optimized by Rietveld refinements [39]. The accuracy of the structure obtained is given by the R-values and the goodness of fit χ. More information on the experimental procedure and analysis is found in Ref. [16] as well as in the literature [40, 43–45].

The following analysis of the data of the δ-phase of Alq$_3$ was made on the assumption that one of the two isomers is the constituent of this phase. First the results for the facial isomer are given, followed by the results for the meridional isomer for comparison.

Figure 12 shows the spectrum observed together with the best Rietveld-fit profiles for the assumption of the facial isomer. The enlarged difference curve between observed and calculated profiles is given in an additional window below. Indexing of this very well resolved powder spectrum with the ITO routine [46] led to a primitive triclinic unit cell for Alq$_3$ with lattice parameters given in Table 2. The number of formula units per unit cell could be determined as $Z = 2$ from packing considerations and density measurements. P-1 was selected as the most probable space group, which was confirmed by Rietveld refinements. The high quality of the refinement becomes obvious from the excellent differential pattern in particular at high diffraction angles (corresponding to small distances in real space), the R_{wp} value of 6.5%, and the Bragg R value R–F^2 of 10.5%. Crystallographic data for δ-Alq$_3$ are listed in Table 2.
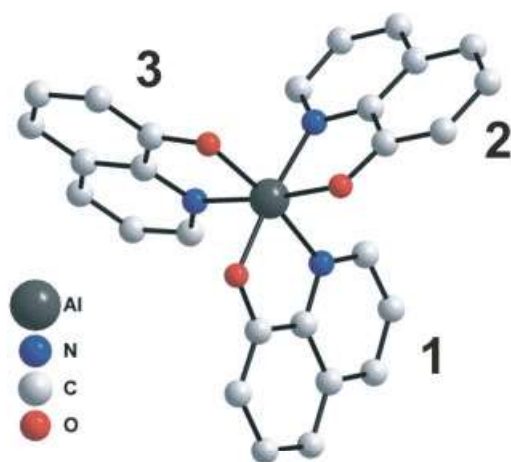
Fig. 13 Facial Alq$_3$ molecule of the δ-phase with the three hydroxyquinoline ligands labeled by 1, 2 and 3. H-atoms are omitted for simplicity.
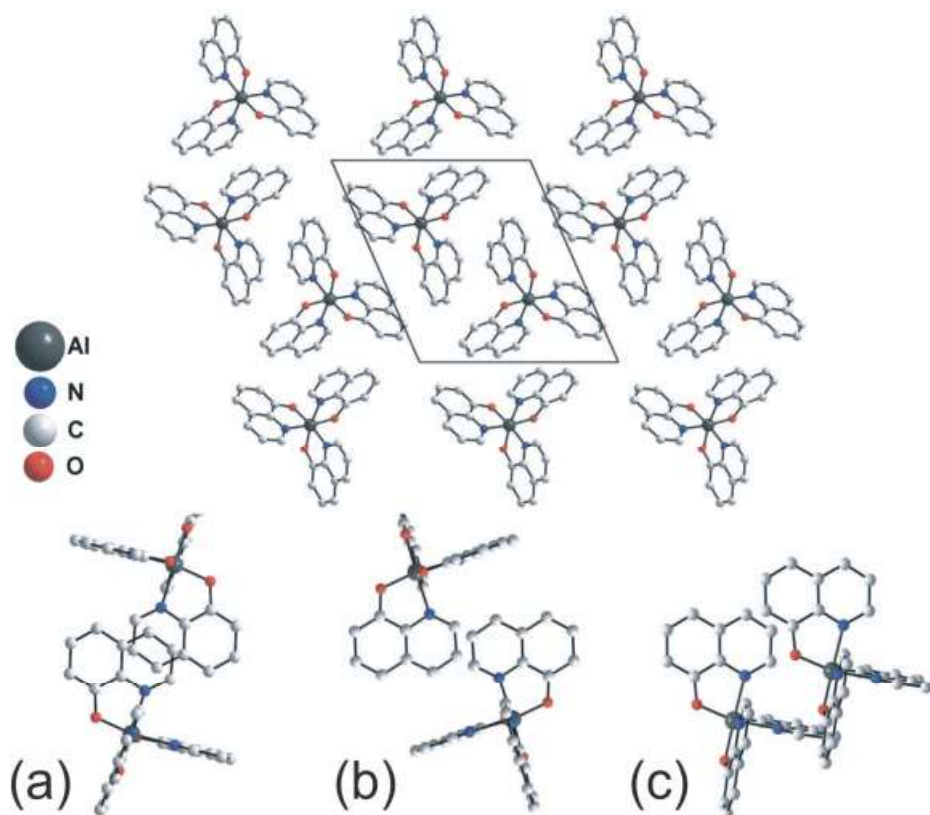
Fig. 14 Crystal structure of □-Alq$_3$ in a projection along the *c*-axis. (a), (b), and (c) are projections perpendicular to the planes of the hydroxyquinoline ligands 1, 2, and 3, respectively, showing the overlap between ligands of neighboring Alq$_3$ molecules.

The molecular structure of δ-Alq$_3$ obtained from these measurements is shown in Fig. 13. Compared to the idealized isolated facial Alq$_3$ isomer, the molecule is only slightly distorted, which reduces its symmetry only negligibly, and the planes defined by the O- and N-atoms, respectively, are parallel. The molecules form linear stacks in the *c*-direction of the crystal. The projection along the *c*-axis as well as the projection perpendicular to the planes of the hydroxyquinoline ligands, which shows the overlap between ligands of neighboring Alq$_3$ molecules, are shown in Fig. 14.

The data was also evaluated on the assumption of the meridional isomer. The best fit obtained for this case is plotted in Fig. 15 together with the differential curve. A comparison with Fig. 12 clearly shows that the fit assuming the meridional isomer is far worse than the result for the facial isomer. Refinement resulted in a distorted meridional molecule, whereby the distance for one coordination bond (Al–N) was elongated more than 10% compared to the others (ligand A and B: ca. 2.1 Å, ligand C: 2.39 Å) and a Bragg *R* value $R–F^2$ of 19.4% was obtained. *R*-Values, tables and a picture of the distorted meridional molecule are given in Ref. [16] and Ref. [52].

The most important outcome of these refinements is that the δ-phase of Alq$_3$ consists of the facial isomer. For a long time it was believed that the facial isomer is unstable and would not exist. Thus the results shown here are the first evidence for the existence of this facial isomer [16, 47]. The simulations assuming the facial isomer closely match the measured spectrum, as can be seen in the differential spectrum in Fig. 12, which is much better than the differential spectrum in Fig. 15 of the best possible fit for the meridional isomer. For the meridional isomer the molecule is distorted and a substantially lower Bragg *R* value (by 9%) was obtained compared to the facial isomer ($R–F^2$ = 10.5% facial, 19.4% merid
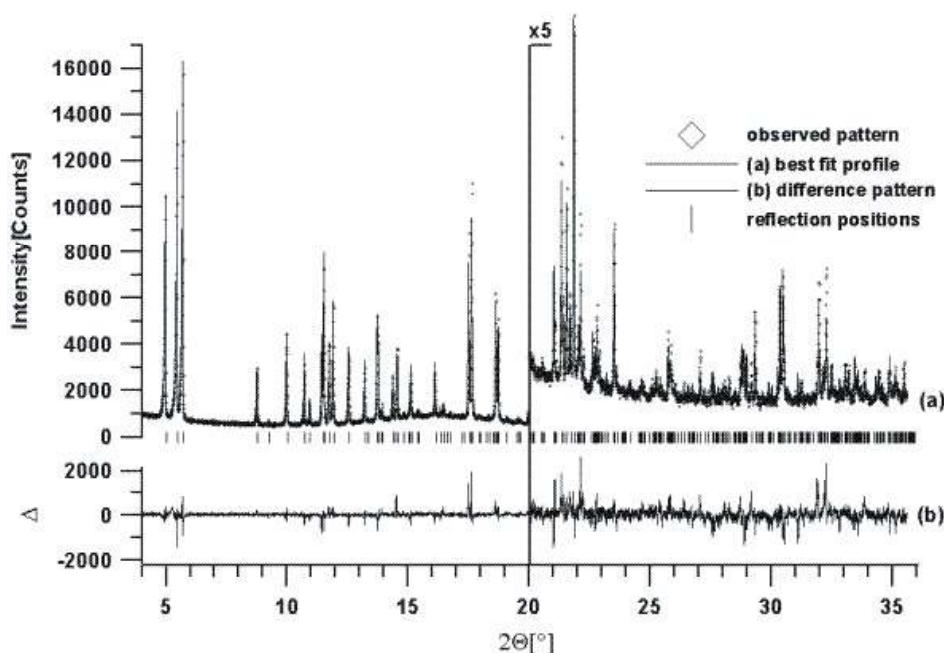
Fig. 15 Scattered X-ray intensity for □-Alq$_3$ at ambient conditions. Shown are the observed patterns (diamonds), the best Rietveld-fit profiles on the assumption of a meridional isomer (line) and the enlarged difference curves between observed and calculated profiles in an additional window below. Best values obtained for R_p, R_{wp} and $R-F^2$ are 7.3%, 9.4% and 19.4%, respectively.

ional). The R values for the facial isomer indicate a high quality of the refinement, resulting in a very high probability that the δ-phase consists of this isomer. Furthermore, the high quality of the fit and the very well resolved spectrum suggests that the samples of δ-Alq$_3$ are an almost pure phase, confirming the results in the previous section. Therefore it can be concluded that the δ-Alq$_3$ samples prepared under defined annealing conditions as described above are a pure phase without significant admixtures of other phases and that δ-Alq$_3$ consists of the facial isomer. Thus, as a result of the preparation of δ-Alq$_3$, we have for the first time successfully isolated the long sought-after facial isomer of Alq$_3$.

This assignment of the facial isomer as being the only constituent of the δ-phase of Alq$_3$ was also very recently confirmed by NMR measurements [50] where the different electric field gradient tensors for the two isomers give characteristic fingerprints for their identification in solid state Al-NMR spectra. Moreover, the group at Eastman Kodak has recently grown single crystals of δ-Alq$_3$ large enough for a single crystal structure analysis. An excellent confirmation of the structure and the packing presented here was obtained [51].

The data also gives information about distance and orientation of the molecules and thus about molecular packing in the crystal. It is noteworthy that the molecules are arranged in a manner minimizing the possible overlap of the π-orbitals between pairs of hydroxyquinoline ligands belonging to neighboring Alq$_3$ molecules, as shown in Fig. 14. As demonstrated by Brinkmann et al., the orbital overlap influences the optical properties and can explain shifts in the photoluminescence spectra of different phases of Alq$_3$ [14]. In δ-Alq$_3$ the pyridine rings of antiparallel ligands 1 face each other with an interligand distance of 3.4 Å (Fig. 14a). The partial overlap of the rings is smaller than in the other known phases, and the atoms are slightly displaced, further reducing the overlap of the π-orbitals. Figure 14b and c show the projection perpendicular to the planes of ligand 2 and ligand 3, respectively. The interligand distance is about 3.45 Å and these ligands do not overlap at all. Thus a strongly reduced π-orbital overlap of neighboring ligands is found in □-Alq$_3$ as compared to the α- and β-phase. As only one ligand of each molecule overlaps with a neighboring molecule, there are no π–π links generating an extended one-

dimensional chain, as reported for the β-phase [14]. In view of this, both the packing effect with reduced intermolecular interaction and the changed symmetry of the molecule are likely to be responsible for the large blue-shift of the photoluminescence by 0.2 eV, which is in the same range as predicted theoretically by Curioni et al. for the two isomers [28].

For transformation from the meridional isomer to the facial isomer one ligand, namely ligand C in Fig. 2, has to flip by 180°. From our results the facial isomer is formed at temperatures above 380 °C; thus the question is of interest whether this transition is energetically allowed for this molecule. Amati et al. made theoretical calculations for several possible transition processes between the geometric isomers of Alq_3 and its stereoisomers, and they found that thermal conversion from the meridional isomer to the facial isomer is energetically possible [48]. Very recently Utz et al. reported on NMR measurements of solutions demonstrating an internally mobile nature of the Alq_3 complex [49]. They found a high probability of ligands flipping by 180° and suggested that this process takes place on a time scale of about $5 \, s^{-1}$ at room temperature in solution. In these measurements they were only able to determine the meridional isomer for two reasons: First, the facial isomer is predicted to be less stable by about 17 kJ/mol for the isolated molecule [28, 48], thereby reducing its lifetime in solution; second, only the flip of ligand C may result in the facial isomer, giving a lower probability for this process, and thus the expected concentration of this isomer in solution is likely to be too small to be measured [49]. These measurements and the theoretical work of Amati et al. demonstrate that the transformation from the meridional isomer to the facial isomer at elevated temperature is possible, as was carried out for the δ-phase.
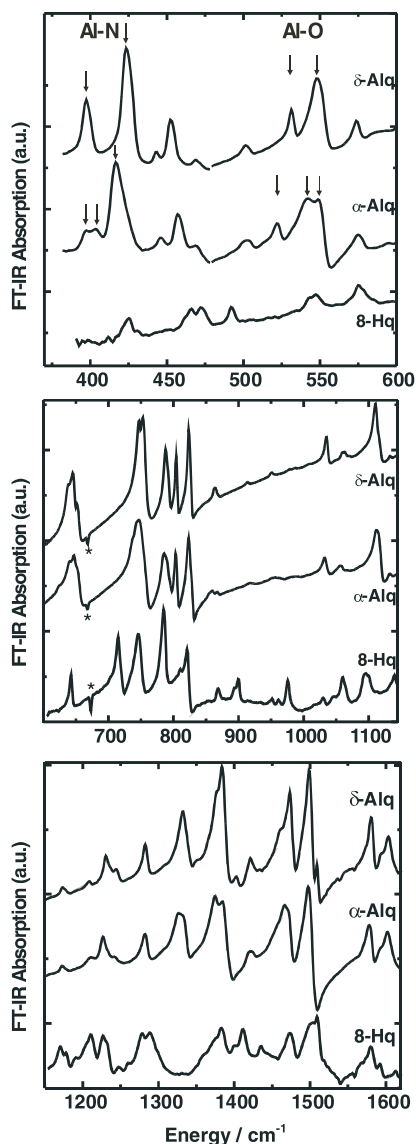
4.2 Vibrational Analysis

Due to the different molecular symmetry of the meridional and facial isomers (C_1 versus C_3), vibrational analysis using infrared (IR) spectroscopy should be another possible method to differentiate between them. In particular, the first coordination sphere or central part of the molecule AlO_3N_3 should show characteristic vibrational properties for each isomer (Al–O and Al–N modes located below 600 cm^{-1}, as calculated by Kushto et al. [25]). Furthermore, there is a weak coupling of the three ligands via the central part, and movements around the central aluminum atom are involved in most of the molecular vibrations below 1700 cm^{-1}. This coupling depends on the relative positions of the oxygen atoms of the ligands (compare Fig. 2). For the facial isomer each

Fig. 16 Comparison of the FTIR-spectra of □-Alq_3 (upper trace), α-Alq_3 (middle trace) and hydroxyquinoline (8-Hq, lower trace) in the range from 350 cm^{-1} to 1650 cm^{-1}.

(a)

C_{2v}

(b)

C_{3v}
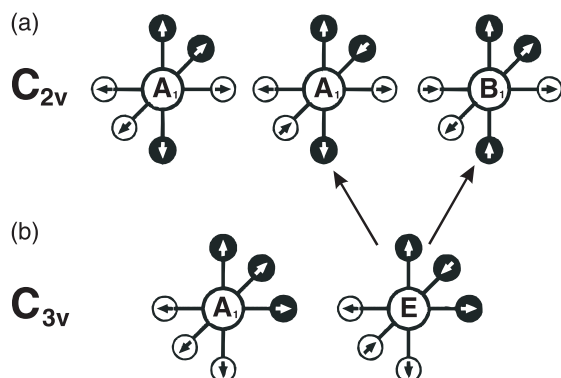
Fig. 17 Schematic picture of the central part of the meridional (a) and the facial (b) isomer of Alq_3. Hollow and filled circles around the central Al-atom represent oxygen and nitrogen atoms, respectively. The three stretching modes of the meridional molecule (C_{2v}-symmetry) and the two for the facial molecule (C_{3v}-symmetry, one is degenerated) are marked by arrows in the O and N atoms.

oxygen atom faces a nitrogen atom, and thus the coupling via the Al atom is identical for all ligands, whereas for the meridional isomer one can clearly distinguish between the ligands labeled by A, B and C in Fig. 2. For the meridional isomer, the coupling mainly affects the ligands B and C, where the oxygen atoms face each other, and to a lesser extent the A and B ligands, which have the oxygen and nitrogen atoms opposite. The coupling mechanism of ligand A and C is mainly characterized by the modes of the two opposite nitrogen atoms. This means that due to the lower symmetry of the meridional molecule each vibrational mode has a slightly different energy for the three ligands.

For the □-phase of Alq_3 it was shown above by structural investigations to consist of the facial isomer. We can therefore use the IR spectra to identify characteristic differences in the vibrational properties of the two isomers. Figure 16 shows a comparison of the FT-IR-spectra of δ-Alq_3, α-Alq_3, and the ligand hydroxyquinoline (8-Hq) alone. In principle one has to distinguish between two regions, above and below 600 cm^{-1}. The lines above 600 cm^{-1} are mainly related to vibrations within the ligands, as one can see from comparison with the 8-Hq spectrum. Due to the different symmetry of the isomers there is a different interaction of the ligands via the Al-atom leading to small differences in this region. The region below 600 cm^{-1} is dominated by the modes of the first coordination sphere or central fragment around the Al-atom. A detailed discussion of these spectra and individual lines as well as a discussion of the influence of crystallinity of the sample can be found in Refs. [47, 52]. In this review we only give the main results and exemplify the discussion by the Al–N and Al–O stretching modes that are marked with arrows in Fig. 16.

If we consider the central fragment AlO_3N_3, the local symmetry for each isomer is C_{2v} and C_{3v}, respectively, as shown in Fig. 17. The separation of the central part from the ligands is justified by the different and well-separated vibrational energies belonging to these groups, as observed in the comparison of Alq_3 with the hydroxyquinoline parent of the ligands in Fig. 16. Particular focus is on the stretching vibrations of this central part. For α-Alq_3, which consists of the meridional isomer (C_{2v}), six stretching vibrations are expected, three involving Al–N and three involving Al–O modes (see Fig. 17). As they are all dipole-allowed, they are observable by IR-spectroscopy. According to Kushto et al. the following assignments for α-Alq_3 are made: Al–N stretching: 396 cm^{-1}, 405 cm^{-1}, 418 cm^{-1}, Al–O stretching: 522 cm^{-1}, 542 cm^{-1}, 549 cm^{-1}. By contrast δ-Alq_3 shows a total of only four bands in this region (397 cm^{-1}, 423 cm^{-1}, 531 cm^{-1}, 548 cm^{-1}). As the AlO_3N_3 fragment of the facial isomer belongs to symmetry C_{3v}, six stretching vibrations are expected here too, but four of them belong to two degenerate vibrational states and therefore only four bands should be observed in IR-spectroscopy, as is the case for δ-Alq_3. The Al–N stretching is found at 397 cm^{-1} and 423 cm^{-1}, the Al–O stretching at 531 cm^{-1} and 548 cm^{-1}. The degeneracy of the first and last band is not present in the α-phase of Alq_3 (see Fig. 16 and Fig. 17), which consists of the meridional isomer. Two lines are observed at 400 cm^{-1} and at 550 cm^{-1} in α-Alq_3, in agreement with theoretical calculations of Kushto et al. [25]. From this and the discussion in Ref. [47] it can be seen, that the analysis of the IR-spectra for the region above as well as below 600 cm^{-1} confirms the presence of the meridional and facial isomer in α-Alq_3 and δ-Alq_3, respectively. Furthermore, the specific fingerprints of the two isomers obtained by IR-spectroscopy may help to identify the isomers in other Alq_3-samples [47].

5 Population and properties of the electronic excited triplet state

5.1 Population of the triplet states

In the previous part of this review structural investigations and properties of the molecule in the electronic ground state were discussed, giving evidence for the existence of the two different geometric isomers. However, not only the electronic ground state should be different for the two isomers, but also the excited states are expected to have different properties due to the different geometry of the molecule. Two types of photoexcited states are distinguished: the singlet state and the triplet state. In the singlet state the total spin quantum number of the unpaired electrons $S = 0$, whereas in the triplet state the total spin quantum number is $S = 1$.

As in most cases the S_0-S_1 transition is an allowed transition, the lifetime of the S_1-state is very short. For Alq$_3$ it was measured to be about 12 ns [3, 29, 53, 54]. On the other hand, the S_0-T_1 transition is a so-called forbidden transition and thus the lifetime of the T_1 state is expected to be several orders of magnitude larger. However, so far very few experimental data on the triplet state of Alq$_3$ have been available, and thus this section includes the first direct measurements of the triplet state. First, a method to investigate the population of the triplet states due to intersystem crossing (ISC) is introduced and applied to discuss the properties of the different phases. Then we briefly discuss very recent results related to the characterization of the electronic excited triplet state in Alq$_3$.

The triplet state T_1 is populated due to intersystem crossing, as schematically shown in Fig. 18. In reality the triplet state splits into three levels $| x \rangle$, $| y \rangle$ and $| z \rangle$. Their energetic distance is characterized by the zero field splitting parameters E and D. To simplify the following discussion this splitting of the triplet state is neglected and only T_1 is given in the schematic Fig. 18. Due to photoexcitation by the absorption of incident laser light, mainly the singlet states S_n are excited ($S_0 \rightarrow S_n$) and relax to the lowest excited singlet state S_1 (process a). The excited singlet state S_1 can relax to the ground state ($S_1 \rightarrow S_0$) by emission of a photon (process b) or simply relax thermally (process c). The triplet state is populated by intersystem crossing with the rate constant d and f is the rate constant for the $T_1 \rightarrow S_0$ transition. In the literature f is often denoted as k_T.

Under constant photoexcitation and for long periods of time ($t \rightarrow \infty$) there is a dynamic equilibrium of the $S_1 \rightarrow T_1$ and $T_1 \rightarrow S_0$ transitions, resulting in a constant concentration of the triplet states $[T_1]^\infty$. The molecules which are in the long-lived triplet state are not able to emit fluorescent light and, at high excitation density, this leads to a decrease in fluorescence intensity. Therefore the process of intersystem crossing can be investigated by transient PL measurements and as a result the ratio of molecules in the triplet state can be estimated. The time dependence of the population process and the concentration of the triplet states $[T_1]^\infty$ is obtained from the rate equations (see Fig. 18):

$$\frac{d[S_0]}{dt} = -a[S_0] + b[S_1] + c[S_1] + f[T_1] , \tag{1}$$

$$\frac{d[S_1]}{dt} = a[S_0] - b[S_1] - c[S_1] - d[S_1] , \tag{2}$$
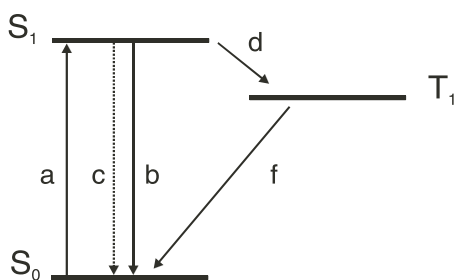
Fig. 18 Schematic diagram of the electron levels and the transitions between the levels in an organic molecule. S_0 and S_1 are the non-excited ground state and the first excited singlet level; T_1 is the lowest triplet level. The coefficient a is proportional to the intensity of the exciting light and the probability of excitation of the molecule. b, c, d and f are the corresponding rate constants. The transition d is the population of the triplet state due to intersystem crossing.

$$\frac{d[T_1]}{dt} = d[S_1] - f[T_1]. \tag{3}$$

These equations were solved by Sveshnikov, and Smirnov et al. [55, 56]. As the rate constants b and c cannot be distinguished experimentally here, they can be replaced by $b' = b + c$. Further, if we bear in mind both that the lifetime of the triplet state is much longer than the lifetime of the singlet state and that the rate of intersystem crossing is much higher than the rate of triplet decay ($b' \gg f$, $d \gg f$), the solutions are

$$[S_1] = \frac{af[S_0]^0}{(b'+d)f+da} + \frac{Aa^2[S_0]^0}{(b'+d)f+da} e^{-\frac{1}{\tau_1}t} - \frac{a[S_0]^0}{b'+d+Ba} e^{-\frac{1}{\tau_2}t}, \tag{4}$$

$$[T_1] = \frac{ad[S_0]^0}{(b'+d)f+da}(1 - e^{-\frac{1}{\tau_1}t}) \tag{5}$$

with

$$f + \frac{d}{b'+d}a = f + Aa = \frac{1}{\tau_1} \tag{6}$$

and

$$b' + d + \frac{b'}{b'+d}a = b' + d + Ba = \frac{1}{\tau_2}. \tag{7}$$

From these equations it is evident that τ_1 is the characteristic time for the accumulation of molecules in the triplet state. For $t \to \infty$ (stationary regime) the concentration of molecules in the triplet state is given by

$$[T_1]^\infty = \frac{ad[S_0]^0}{(b'+d)f+da} = Aa[S_0]^0\tau_1 \tag{8}$$

and finally with Eq. (6) one can express $[T_1]^\infty$ by the characteristic accumulation time τ_1 and the lifetime of the molecules in the triplet state $\tau_0 = 1/f$.

$$[T_1]^\infty = [S_0]^0\left(1 - \frac{\tau_1}{\tau_0}\right). \tag{9}$$

As a result it is possible to estimate the ratio of the molecules excited in the triplet state $[T_1]^\infty$ from the lifetime τ_0, determined from delayed fluorescence measurements that will be discussed below, and the characteristic accumulation time τ_1, which can be measured using transient PL studies.

These measurements for the Alq$_3$ phases as well as for an evaporated amorphous film are shown in Fig. 19. Instantaneously with the turning-on of the excitation light the fluorescence is observed, which subsequently decreases with a decay time τ_1 to an equilibrium value. α-Alq$_3$, yellowish-green Alq$_3$ and the evaporated amorphous film behave in a similar fashion. Their decay time τ_1 is 11 ms, 11 ms, and 7 ms, and the triplet lifetime τ_0 at that temperature (1.3 K) was measured as 15 ms, 14 ms, and 9 ms respectively. Therefore in these samples about 20% to 30% of the molecules are in the triplet state. This similarity between these samples of Alq$_3$ containing the meridional isomer is remarkable, because it clearly demonstrates that the morphology and thus intermolecular interactions seem to have no signifi-

1112
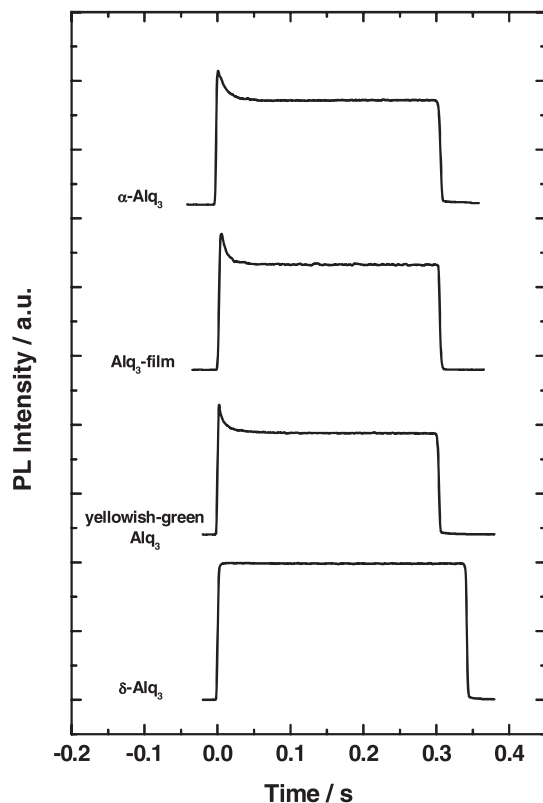
Fig. 19 Time dependence of the PL-intensity during an optical excitation pulse for polycrystalline Alq_3 phases and an evaporated film. The measurements were performed at 1.3 K by using excitation at 363.8 nm. The signal was detected at 2.64 eV (470 nm) for δ-Alq_3 and at 2.48 eV (500 nm) for all other samples.

cant influence on the intersystem crossing process in Alq_3. However, for δ-Alq_3 there is only a very small decrease in the PL intensity and the equilibrium value remains at 98%. Due to the small decay and the noise of the measurement, the error for determination of τ_1 is too large, but from the decrease in intensity one may roughly estimate that only about 2% of the molecules in δ-Alq_3 are in the triplet state. From the independence of the morphology of the samples it can be concluded that the low population of the triplet state due to strongly reduced intersystem crossing is a molecular property of the facial isomer in δ-Alq_3. This has also been confirmed recently by Amati et al. using quantum chemical calculations [57].

5.2 Phosphorescence of Alq_3

While the measurement of the transient PL discussed above only gives information about intersystem crossing to the triplet state but not its energetic position and lifetime, we have recently succeeded in obtaining this information by directly detecting light emission from the triplet state to the singlet ground state in Alq_3. The phosphorescence was found in the spectrum of the delayed luminescence at low temperatures as shown in Fig. 20. This spectrum consists of one band located at about 525 nm and a second band at 700 nm. The band at 525 nm is the delayed fluorescence which occurs due to a T–T annihilation process [58]. The second band with a maximum at 700 nm is the phosphorescence of Alq_3. Both bands can be used for the determination of the triplet lifetime τ_0, which was found to be about 16 ms at this temperature. We have seen phosphorescence for all crystalline phases and also for evaporated amorphous films. As reported recently, the phosphorescence of Alq_3 can also be observed in OLEDs [59]. Moreover it was shown that free hydroxyquinoline ligands have no effect on the spectrum shown in Fig. 20 [52]. A detailed discussion of these new results will be presented in a forthcoming publication [60].
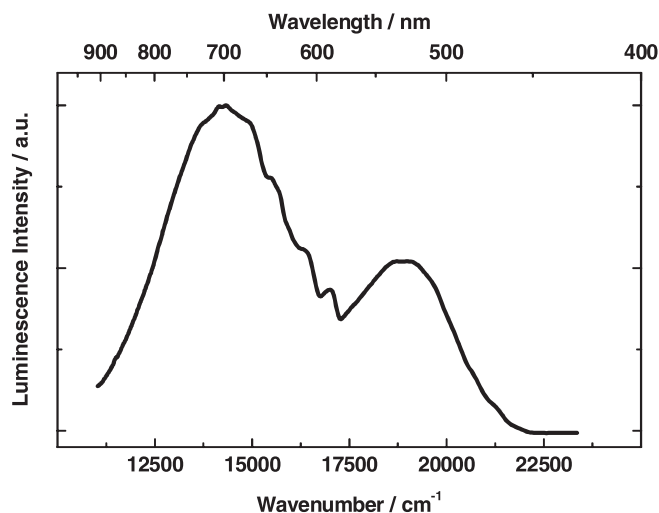
Fig. 20 Delayed luminescence spectrum of α-Alq$_3$ measured 4ms after the end of the laser pulse at 10 K. The spectrum consists of two distinct bands, the delayed fluorescence with a maximum at about 525 nm and the phosphorescence at about 700 nm. The vibronic progressions are clearly resolved on the high energy side of the phosphorescence.

6 Summary

In this review we have presented detailed investigations on polycrystalline Alq$_3$-samples prepared using sublimation in a horizontal glass tube with a temperature gradient or by annealing. The thermal, structural and photophysical properties were investigated by using differential scanning calorimetry (DSC), X-ray diffraction, infrared spectroscopy, and photoluminescence measurements, with the focus on the comparison of the different phases.

It was shown that different fractions of Alq$_3$ can be separated in the sublimation tube; they differ in the shape of the crystals, their color, their solubility, and their fluorescence. An important outcome was the discovery of a new blue luminescent crystalline phase of Alq$_3$ (δ-Alq$_3$), which has significantly different properties compared to all other known phases (α, β, γ). Furthermore, it was demonstrated that the material commonly used for the evaporation of thin films in OLEDs (here named yellowish-green Alq$_3$) mainly consists of α-Alq$_3$ with some small admixtures of δ-Alq$_3$.

As temperature has a strong influence on the formation of these polycrystalline phases, the formation conditions of the different phases of Alq$_3$ were investigated using differential scanning calorimetry measurements in combination with structural and optical characterization. As a result a phase transition at about 380 °C was identified where blue luminescent Alq$_3$ is formed. From detailed investigations of the processes in the temperature region between 385 °C and 410 °C, the two high-temperature phases δ-Alq$_3$ and γ-Alq$_3$ were identified. In addition, an efficient method was developed to prepare large amounts (several grams) of pure blue luminescent δ-Alq$_3$. It was also shown that all phases can easily be transformed into each other; thus chemical reactions could be excluded.

Well-defined preparation of pure δ-Alq$_3$ was the prerequisite for high resolution X-ray measurements on δ-Alq$_3$ powder including structural refinements. The high quality of these refinements gave convincing evidence that the facial isomer constitutes the δ-phase of Alq$_3$. The data also provided information about distance and orientation of the molecules and thus about molecular packing in the crystal. Compared to the α- and β-phase, both consisting of the meridional isomer, a strongly reduced π-orbital overlap of hydroxyquinoline ligands belonging to neighboring Alq$_3$ molecules was found in □-Alq$_3$. Therefore both the packing effect with reduced intermolecular interaction and the changed symmetry of the molecule are likely to be responsible for the large blue-shift of the photoluminescence.

Using infrared spectroscopy it was demonstrated how the isomerism of the Alq$_3$ molecule is manifested in the vibrational properties. Comparison of the experimental results with theoretical calculations provided further evidence of the presence of the facial isomer in the blue luminescent δ-phase of Alq$_3$.

Finally this article presented first results of the electronic excited triplet state in Alq_3. The intersystem crossing behavior was investigated and the phosphorescence spectrum was measured for the first time and it was found that the reduced population of the triplet states in δ-Alq_3 due to intersystem crossing is a characteristic property of the facial isomer.

With regard to the application of Alq_3 in OLEDs, it is important to note that the simple annealing process can be used to obtain thin films of blue luminescent Alq_3. In preliminary experiments evaporated amorphous thin films with thicknesses from 300 nm to 15 μm, were encapsulated and converted at 390 °C into thin films showing blue luminescence. In addition it was possible to evaporate blue luminescent thin films directly onto heated glass substrates. At present these films are still comparatively thick (several microns), have polycrystalline structure, and need further optimization. This would then allow OLEDs to be manufactured with blue luminescent δ-Alq_3. Further work to characterize such films and their application in OLEDs is in progress.

References

[1] W. Ohnesorge and L. Rogers, Spectrochim. Acta, Part A **15**, 27 (1959).
[2] C. Tang and S. VanSlyke, Appl. Phys. Lett. **51**, 913 (1987).
[3] C. Tang and S. VanSlyke, J. Appl. Phys. **65**, 3610 (1989).
[4] J. Shi and C. Tang, Appl. Phys. Lett. **70**, 1665 (1997).
[5] L. Hung, C. Tang, and M. Mason, Appl. Phys. Lett. **70**, 152 (1997).
[6] H. Aziz, Z. Popovic, N.-X. Hu, A. Hor, and G. Xu, Science **283**, 1900 (1999).
[7] H. Kubota, S. Miyaguchi, S. Ishizuka, T. Wakimoto, J. Funaki, Y. Fukuda, T. Watanabe, H. Ochi, T. Sakamoto, T. Miyake, M. Tsuchida, I. Ohshita, and T. Tohma, J. Lumin. **87–89**, 56 (2000).
[8] T. Tsutsui, M. Yang, M. Yahiro, K. Nakamura, T. Watanabe, T. Tsuji, Y. Fukuda, T. Wakimoto, and S. Miyaguchi, Jpn. J. Appl. Phys. 2, **38**, 1502 (1999).
[9] P. Burrows, Z. Shen, V. Bulovic, D. McCarty, S. Forrest, J. Cronin, and M. Thompson, J. Appl. Phys. **79**, 7991 (1996).
[10] S. Barth, U. Wolf, H. Bässler, P. Müller, H. Riel, H. Vestweber, P. Seidler, and W. Rieß, Phys. Rev. B **60**, 8791 (1999).
[11] M. Stößel, J. Staudigel, F. Steuber, J. Blässing, J. Simmerer, and A. Winnacker, Appl. Phys. Lett. **76**, 115 (2000).
[12] W. Brütting, S. Berleb, and A. Mückl, Organic Electronics **2**, 1 (2001).
[13] S. Berleb and W. Brütting, Phys. Rev. Lett. **89**, 286601 (2002).
[14] M. Brinkmann, G. Gadret, M. Muccini, C. Taliani, N. Masciocchi, and A. Sironi, J. Am. Chem. Soc. **122**, 5147 (2000).
[15] M. Braun, J. Gmeiner, M. Tzolov, M. Cölle, F. Meyer, W. Milius, H. Hillebrecht, O. Wendland, J. von Schütz, and W. Brütting, J. Chem. Phys. **114**, 9625 (2001).
[16] M. Cölle, R. E. Dinnebier, and W. Brütting, Chem. Commun. **23**, 2908 (2002).
[17] M. Cölle, J. Gmeiner, W. Milius, H. Hillebrecht, and W. Brütting, Adv. Funct. Mater. **13**, 108 (2003).
[18] G. Kauffmann, Coord. Chem. Rev. **12**, 105 (1974).
[19] R. Larsson and O. Eskilsson, Acta Chem. Scand. **22**, 1067 (1968).
[20] B. C. Baker and D. T. Sawyer, Anal. Chem. **40**, 1945 (1968).
[21] J. Majer and M. Reade, Chem. Commun. **1**, 58 (1970).
[22] M. Halls and R. Aroca, Can. J. Chem. **76**, 1730 (1998).
[23] N. Johansson, T. Osada, S. Stafström, W. Salaneck, V. Parente, D. dos Santos, X. Crispin, and J. Brédas J. Chem. Phys. **111**, 2157 (1999).
[24] R. Martin, J. Kress, I. Campbell, and D. Smith, Phys. Rev. B **61**, 15804 (2000).

[25] G. Kushto, Y. Iizumi, J. Kido, and Z. Kafafi, J. Phys. Chem. A **104**, 3670 (2000).
[26] M. Ichikawa, H. Yanagi, Y. Shimizu, S. Hotta, N. Suganuma, T. Koyama, and Y. Taniguchi, Adv. Mater. **14**, 1272 (2002).
[27] R. J. Curry, W. P. Gillin, J. Clarkson, and D. N. Batchelder, J. Appl. Phys. **92**, 1902 (2002).
[28] A. Curioni, M. Boero, and W. Andreoni, Chem. Phys. Lett. **294**, 263 (1998).
[29] W. Humbs, H. Zhangand, and M. Glasbeek, Chem. Phys. **254**, 319 (2000).
[30] J. Steiger, R. Schmechel, and H. von Seggern, Synth. Met. **129**, 1 (2002).
[31] E. Ito, Y. Washizu, N. Hayashi, H. Ishii, N. Matsuie, K. Tsuboi, Y. Ouchi, Y. Harima, K. Yamashita, and K. Seki, J. Appl. Phys. **92**, 7306 (2002).
[32] M. Amati and F. Lelj, J. Phys. Chem. A **107**, 2560 (2003).
[33] M. Muccini (private communication).
[34] L. S. Sapochak, A. Padmaperuma, N. Washton, F. Endrino, G. T. Schmett, J. Marshall, D. Fogarty, and S. R. Forrest J. Am. Chem. Soc. **123**, 6300 (2001).
[35] Mettler-Toledo, User Comm. **11**, 4 (2000).
[36] B. Wunderlich (1990), Thermal Analysis. Academic Press, San Diego.
[37] J. Ford and P. Timmins, (1989). Pharmaceutical Thermal Analysis.
[38] K. Naito and A. Miura, J. Phys. Chem. **97**, 6240 (1993).
[39] H. Rietveld, J. Appl. Cryst. **2**, 65 (1969).
[40] L. Langford and D. Louer, Rep. Prog. Phys. **59**, 131 (1996).
[41] R. Young and D. Wiles J. Appl. Cryst. **15**, 430 (1982).
[42] R. J. Hill and R. X. Fischer, J. Appl. Cryst. **23**, 462 (1990).
[43] W. Massa (2000), Crystal structure determination. Springer, Berlin.
[44] R. Young (1993), The Rietveld Method. Oxford University Press, New York.
[45] P. Coppens (1992), Synchrotron Radiation Crystallography. Academic Press, London.
[46] J. W. Visser, J. Appl. Cryst. **2**, 89 (1969).
[47] M. Cölle, S. Forero-Lenger, J. Gmeiner, and W. Brütting, Phys. Chem. Phys. **5**, 2958 (2003).
[48] M. Amati and F. Lelj, Chem. Phys. Lett. **363**, 451 (2002).
[49] M. Utz, C. Chen, M. Morton, and F. Papadimitrakopoulos, J. Am. Chem. Soc. **125**, 1371 (2003).
[50] M. Utz, M. Nandagopal, M. Mathai, and F. Papadimitrakopoulos, Appl. Phys. Lett. **83**, 4023 (2003).
[51] M. Rajeswaran, T. N. Blanton, and K. P. Klubek, Z. Kristallogr. NCS **218**, 439 (2003).
[52] M. Cölle (2004), The Electroluminescent Material Alq$_3$, Logos, Berlin.
[53] T. Mori, K. Obata, K. Miyachi, T. Mizutani, and Y. Kawakami, Jpn. J. Appl. Phys. 1 **36**, 7239 (1997).
[54] Y. Kawasumi, I. Akai, and T. Karasawa, Int. J. Mod. Phys. B **15**, 3825 (2001).
[55] B. Sveshnikov, Z. Eksp. Teo. Fiz. **18**, 878 (1948).
[56] V. Smirnov and M. Alfimov, Kinetika i Kataliz **7**, 583 (1966).
[57] M. Amati and F. Lelj, Chem. Phys. Lett. **358**, 144 (2002).
[58] C. E. Pope and M. Swenberg, (1982), Electronic processes in organic crystals. Clarendon Press, Oxford.
[59] M. Cölle and C. Gärditz, Appl. Phys. Lett. **84**, 3160 (2004).
[60] M. Cölle et al., manuscript in preparation.